

## Supporting information

### Hierarchical $\text{Cu}_{0.27}\text{Co}_{2.73}\text{O}_4/\text{MnO}_2$ nanorod arrays grown on 3D nickel foam as promising electrode materials for electrochemical capacitors

Hongwei Ge, Chengxiang Wang, Longwei Yin\*

Key Laboratory for Liquid-Solid Structural Evolution and Processing of Materials, Ministry of Education, School of Materials Science and Engineering, Shandong University, Jinan 250061, P. R. China

Email: [yinlw@sdu.edu.cn](mailto:yinlw@sdu.edu.cn)

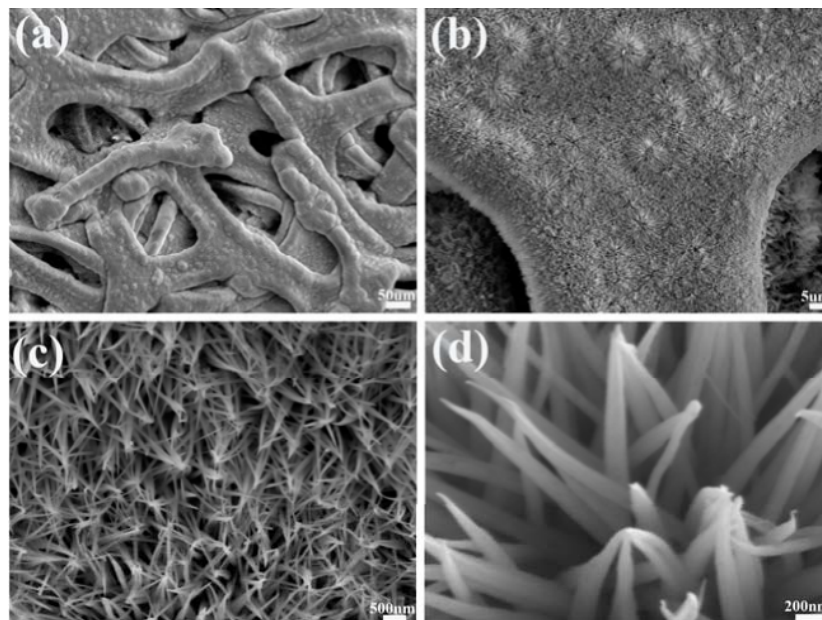


**Fig. S1.** SEM images of precursor to  $\text{Cu}_{0.27}\text{Co}_{2.73}\text{O}_4$  with different magnifications.

**Fig. S1** Shows the different magnified SEM images of the precursor to  $\text{Cu}_{0.27}\text{Co}_{2.73}\text{O}_4$  grown on the nickel foam.

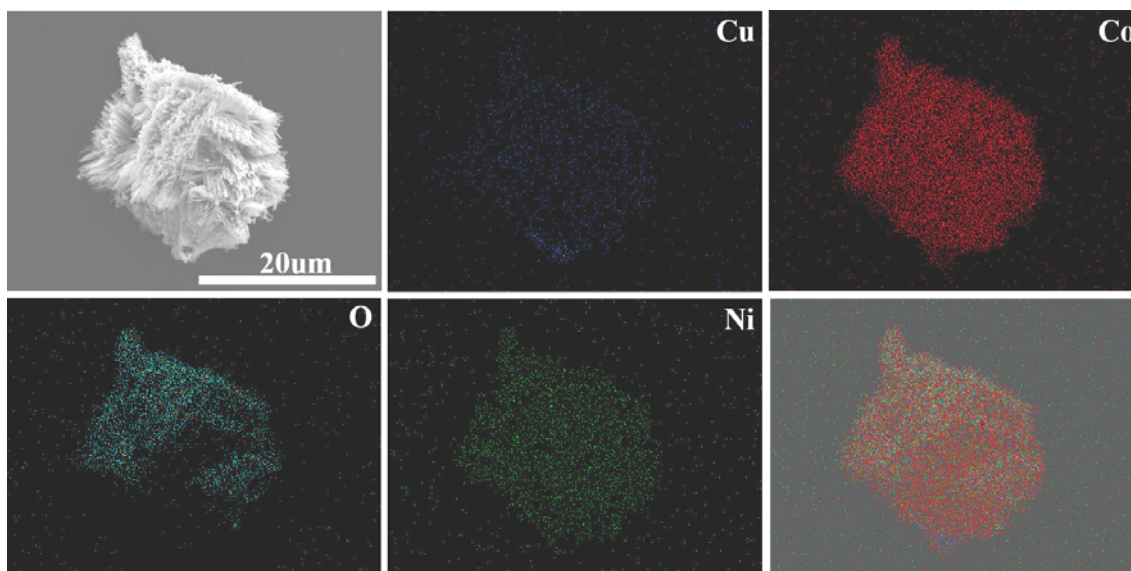


**Fig. S2.** Energy dispersive X-ray spectrometry mapping analysis of  $\text{Cu}_{0.27}\text{Co}_{2.73}\text{O}_4$ , and combined map of the existent elements.

The elements composition of  $\text{Cu}_{0.27}\text{Co}_{2.73}\text{O}_4$  were further determined by Energy Dispersive X-ray spectrometry mapping analysis, shown in **Figure S2**.

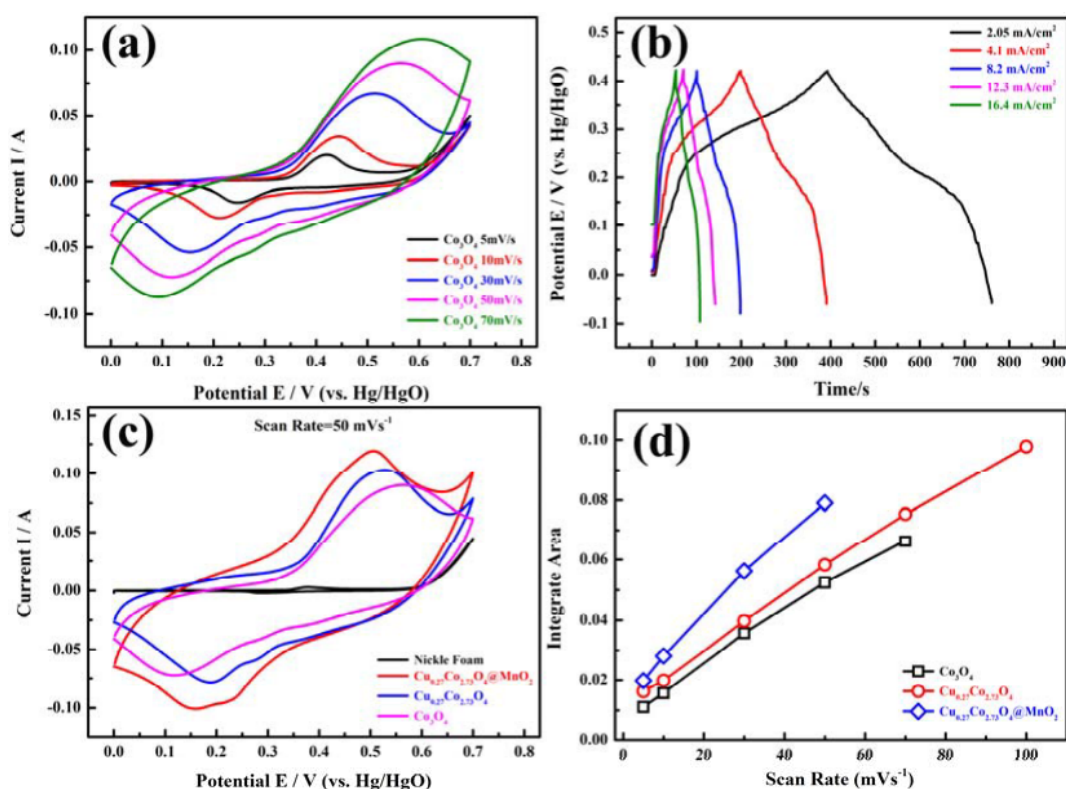


**Fig. S3.** (a) CV curves of  $\text{Co}_3\text{O}_4$  at different scan rates, (b) Galvanostatic charge-discharge (GCD) curves of  $\text{Co}_3\text{O}_4$  at different current densities (within the potential window from -0.05 to 0.42V), (c) CV curves for  $\text{Cu}_{0.27}\text{Co}_{2.73}\text{O}_4$ ,  $\text{Cu}_{0.27}\text{Co}_{2.73}\text{O}_4@\text{MnO}_2$ ,  $\text{Co}_3\text{O}_4$  and nickel foam at a scan rate of  $50 \text{ mVs}^{-1}$  (d) The integrate area of CV curves versus scan rates for  $\text{Cu}_{0.27}\text{Co}_{2.73}\text{O}_4$  and  $\text{Cu}_{0.27}\text{Co}_{2.73}\text{O}_4@\text{MnO}_2$ .

The CV measurement for  $\text{Co}_3\text{O}_4$  is conducted at different scan rates from 5 to  $70 \text{ mVs}^{-1}$  within 0-0.7V. A pair of expanded redox peaks is observed and all profiles exhibits the similar shapes. As the scan rate increases, the

current density and integral area of the CV curves increase., as in Fig. S3.(a) shown. The mass loading of  $\text{Co}_3\text{O}_4$  is  $\sim 4.1\text{mgcm}^{-2}$ . GCD curves of  $\text{Co}_3\text{O}_4$  also rely on the GCD profiles (Fig. S3.(b) shows), we figure out the capacitance through eq. 6 and 7. The capacitance at different current densities (from 2.05 to  $16.4\text{mAcm}^{-2}$ ) is 1.85, 1.80, 1.77, 1.74, 1.67  $\text{Fcm}^{-2}$ , respectively.  $C_a$  of  $\text{Cu}_{0.27}\text{Co}_{2.73}\text{O}_4$  at 2.2, 4.4, 8.8, 13.2,  $17.6\text{mAcm}^{-2}$ , is 2.73, 2.68, 2.42, 2.33,  $2.24\text{Fcm}^{-2}$ , while  $C_a$  of  $\text{Cu}_{0.27}\text{Co}_{2.73}\text{O}_4/\text{MnO}_2$  at 3.1, 6.2, 12.4, 18.6 and  $24.8\text{mAcm}^{-2}$  is 3.40, 3.35, 3.27, 3.13 and  $3.10\text{Fcm}^{-2}$ , respectively. Both of them are much higher than those of  $\text{Co}_3\text{O}_4$ .  $\sim 90\%$  of  $C_a$  retained when current density increases from 2.05 to  $16.4\text{mAcm}^{-2}$  for  $\text{Co}_3\text{O}_4$ , exhibiting excellent rate capability.

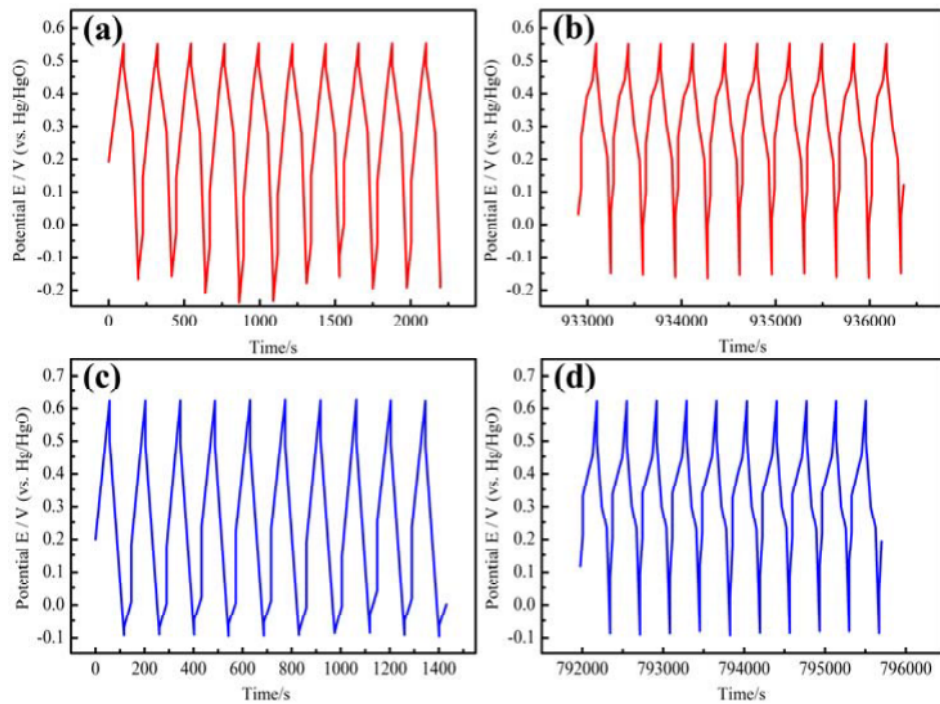


**Fig. S4.** (a) The first 10 and (b) last 10 charge-discharge curves during 3000 cycles for  $\text{Cu}_{0.27}\text{Co}_{2.73}\text{O}_4$  at  $8.8\text{mAcm}^{-2}$ ; (c) The first 10 and (d) last 10 charge-discharge curves during 3000 cycles for  $\text{Cu}_{0.27}\text{Co}_{2.73}\text{O}_4/\text{MnO}_2$  at  $18.6\text{mAcm}^{-2}$ .